Effects of breathing and oblong mode phonons on transport properties in a single-electron transistor

2010 J. Phys.: Condens. Matter 22 065301

(http://iopscience.iop.org/0953-8984/22/6/065301)

J. Phys.: Condens. Matter **22** (2010) 189801 (1pp) doi:10.1088/0953-8984/22/18/189801

Erratum

Effects of breathing and oblong mode phonons on transport properties in a single-electron transistor

Norihiko Nishiguchi and Martin N Wybourne

2010 *J. Phys.: Condens. Matter* **22** 065301

It has come to the attention of the authors that an error occurred in figure 3 of the above paper. An additional line appears below the $T = 4$ line which should not be there. The corrected figure is as follows:

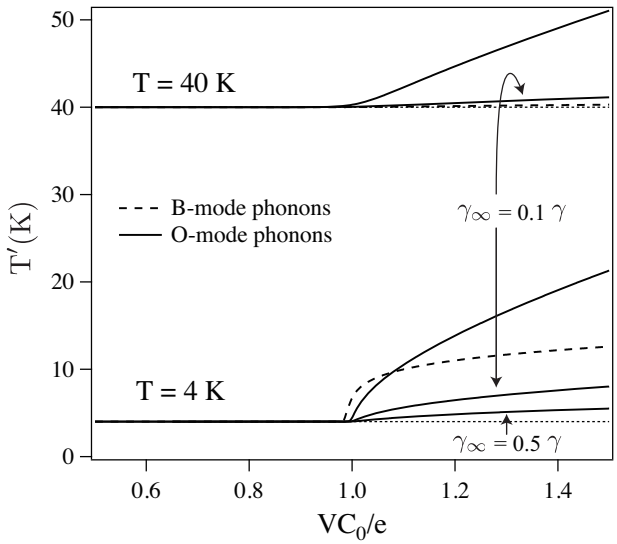

Figure 3. The temperature T' in the nanoparticle versus V at $T = 4$ K for $\gamma_\infty = 0.01\gamma$, 0.1γ and 0.5γ. The data lines of $\gamma_\infty = 0.1\gamma$ and 0.5γ are denoted by arrows. T is the temperature of the heat bath.

IOP Publishing Journal of Physics: Condensed Matter

J. Phys.: Condens. Matter **22** (2010) 065301 (12pp) doi:10.1088/0953-8984/22/6/065301

Effects of breathing and oblong mode phonons on transport properties in a single-electron transistor

Norihiko Nishiguchi[1] **and Martin N Wybourne**[2]

[1] Department of Applied Physics, Hokkaido University, Sapporo 060-8628, Japan
[2] Department of Physics and Astronomy, Dartmouth College, Hanover, NH 03755, USA

E-mail: nn@eng.hokudai.ac.jp and martin.n.wybourne@dartmouth.edu

Received 11 November 2009
Published 27 January 2010
Online at stacks.iop.org/JPhysCM/22/065301

Abstract

We investigate theoretically the transport characteristics of a single-electron transistor affected by the dynamic deformation of the device configuration due to phonons. By considering changes in capacitances and tunnel resistances caused by the breathing and oblong vibrations of the island that forms part of the transistor, we formulate the electron–phonon interaction peculiar to the device and derive its transport properties by means of the master equation. For a single electron transistor with a gold nanoparticle island of radius 1 nm, we demonstrate the contribution to the transport properties that originates from tunneling channels associated with THz phonon emission and absorption.

1. Introduction

It is well known that electron–phonon interactions affect the electronic states in a solid, which leads to a rich variety of transport phenomena. It is also well established that the transport properties of nanoscale electronic devices can depend on the geometry of the system. A useful tool for investigating the geometry and the electronic structure in molecular junctions is inelastic electron tunneling that occurs as a consequence of electron–phonon interactions in the junction [1, 2].

In molecular devices, electron tunneling couples with vibrations of molecules in two ways [3]; electron tunneling induces internal vibrations owing to rearrangement of the atomic configuration, and the charged molecules are driven in the bias electric field. The coupling between the vibrations and tunneling cause phonon-mediated electron transport channels, giving rise to characteristic I–V curves owing to multi-phonon emission and absorption [4–8].

The effect of phonons on the electron transport properties of a metal-based single-electron transistor (SET) is more limited since the nanoparticle is too stiff to allow the atomic configuration changes in accordance with tunneling like the molecular devices, and then phonons do not couple with electron tunneling. For such devices operated in the Coulomb blockade regime, the electron–phonon interaction causes electron energy fluctuations that, based on the bulk electron–phonon interaction, are independent of the system size. Hence, except for the translational vibrations of molecules, electron transport characteristics that reflect multi-phonon emission and absorption are not expected in the device.

In spite of that, we anticipate phonon-mediated transport properties similar to the molecular devices due to a different type of electron–phonon interaction. The nanoparticle island is positioned in the vicinity of the electrodes, where the gaps between the island and electrodes set the key electronic parameters for the SET; the capacitances and tunnel resistances. Surface displacement of the particle island due to phonons modifies the gaps, which is expected to remarkably affect the current through the SET.

In this paper we investigate the effects of gap modulation on the electron transport in the SET. To understand the character and magnitude of possible phonon effects, we consider an ideal SET containing a metal nanoparticle between the source and drain (figure 1). Such a system might be realized by attaching the particle to the electrodes with biomolecules such as RNA or DNA [9]. The metal island is assumed to be a sphere that supports a variety of acoustic phonon modes (see appendix A). The particle has an almost stress-free surface and will have relatively large amplitude surface vibrations due to phonons. In particular, only the breathing modes of spherical symmetry change the intrinsic capacitance of the island and

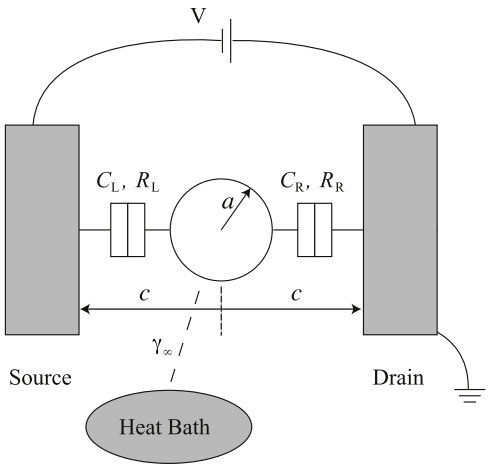

Figure 1. Model of a SET. The nanometal particle is linked electrically to the source and drain made of conducting planes. $C_{L(R)}$ and $R_{L(R)}$ are the capacitance and tunnel resistance between the particle and the left (right) electrode, respectively. a and c are the radii of the metal particle and the distance between the particle and the leads. The oval below the particle indicates a heat bath.

the oblong modes modify tunnel resistances significantly more than other modes, as discussed below. Considering these, we investigate the contributions of breathing and oblong mode phonons to the transport, respectively, as the representative cases.

Thanks to the nature of the attachment, the particle might move in a shuttle fashion between the electrodes [10–20]. This translational shuttle motion also changes the capacitances and tunnel resistances. In order to differentiate these effects from those of surface vibrations, we will assume the particle to be firmly fixed centrally between the electrodes. We also note that the system considered here is different to that of an SET used in a nanoelectromechanical system as a means to transduce the subtle motion of a nanoresonator [21–25]. In that situation the SET itself is taken to have rigid components and the transduction generally occurs via modulation of the coupling capacitance between the resonator and the SET island [22].

This paper is planned as follows; in section 2, we describe the system to be studied in this work and introduce the Hamiltonian of the system. The phonon-mediated tunneling is formulated in this section. In section 3, dealing with the phonon-mediated tunneling as a perturbation, the non-perturbed part of the Hamiltonian is diagonalized by means of a canonical transform. In section 4, the density matrix and associated master equations are introduced. In section 5, we give numerical results for the thermal and transport properties. Finally, section 6 provides a discussion and summary of the work. Derivation of acoustic phonon modes in the particle is given in the appendices.

2. Model

We consider an SET containing a gold spherical particle a in radius, which is suspended centrally between the source and drain made of conducting planes (figure 1). The electron transport is due to single-electron tunneling between the metal particle and the electrodes in the Coulomb blockade regime. The metal particle is connected to a heat bath, whose coupling strength is γ_∞. Although the heat bath is depicted separately from the electrodes in figure 1, the electrodes may act as the heat bath.

The Hamiltonian H of the SET is given by

$$H = H_L + H_R + H_D + H_T + H_{ph} + H_b + H_{ph\text{-}b}, \quad (1)$$

where H_L, H_R and H_D are the Hamiltonians of electrons in the source, the drain and the particle, respectively, and H_T is the tunnel Hamiltonian:

$$H_L = \sum_k (\varepsilon_{L,k} + eV) c^\dagger_{L,k} c_{L,k} \quad (2)$$

$$H_R = \sum_k \varepsilon_{R,k} c^\dagger_{R,k} c_{R,k} \quad (3)$$

$$H_D = \sum_k \left(\varepsilon_{D,k} + \frac{eV}{2}\right) c^\dagger_{D,k} c_{D,k} + \frac{e^2}{2C(r)} \left(\sum_k c^\dagger_{D,k} c_{D,k}\right)^2 \quad (4)$$

$$H_T = \exp\left(\frac{r-a}{\lambda}\right) \sum_{k,k'} \left[t^0_L c^\dagger_{L,k} c_{D,k'} + t^{0*}_L c^\dagger_{D,k'} c_{L,k} + t^0_R c^\dagger_{R,k} c_{D,k'} + t^{0*}_R c^\dagger_{D,k'} c_{R,k}\right]. \quad (5)$$

In equations (2)–(5), $c^\dagger_{\alpha,k}$ and $c_{\alpha,k}$ are the creation and annihilation operators, and $\varepsilon_{\alpha,k}$ is the energy of an electron of k-state. The subscript α means the source for $\alpha = L$, the drain for $\alpha = R$ and the particle for $\alpha = D$. V is the bias voltage and $e(>0)$ is the elementary charge. t^0_α in H_T (equation (5)) is the coefficient of tunneling and the factor $\exp(\frac{r-a}{\lambda})$ is introduced to express the modulation of tunnel resistance, considering that both the breathing and oblong modes expand or shrink the left and right gaps between the island and leads simultaneously. Here r is the radius of the particle, including the surface displacement u_r due to phonons:

$$r = a + u_r, \quad (6)$$

and λ is a characteristic length of tunneling.

For the breathing mode phonons, r is independent of solid angles and then the nanoparticle remains a sphere after deformation. We estimate the capacitance between a metal sphere and a conducting plane, using the method of images [26], as

$$C_{sphere}(r) = 4\pi\varepsilon^*\varepsilon_0 r \left(1 + \alpha + \frac{\alpha^2}{1-\alpha^2} + \cdots\right), \quad (7)$$

where $\alpha = \frac{r}{2c}$. Here c is the distance between the center of the particle and the conducting plane, and then $\alpha < \frac{1}{2}$. The total capacitance $C(r)$ in equation (4) of the SET is composed of C_L and C_R, each of which is given by equation (7). Since the particle is positioned at the midpoint between the source and drain, $C_L = C_R$ and then the total capacitance becomes twice equation (7), i.e. $C(r) = 2C_{sphere}(r)$. For a small displacement in comparison with radius, i.e. $|u_r| \ll a$, $C(r)$ is approximated as

$$\frac{1}{C(r)} \approx \left(1 - \beta\frac{u_r}{a}\right)\frac{1}{C_0}, \quad (8)$$

where $C_0 = C(a)$ and the factor β is defined by

$$\beta = 1 + \frac{a}{2c}. \tag{9}$$

It is known that the intrinsic capacitance of a substance with finite volume is a minimum for a sphere [27]. Then the change in the intrinsic capacitance for the oblong modes depends on u_r^2 and the change in the capacitance is mainly due to the change in the gaps between the island and electrodes. Considering only the change in α in equation (7), we obtain

$$\beta = \frac{a}{2c}, \tag{10}$$

where we suppose that the sphere is stretched toward the electrodes and regard u_r as the surface displacement in the direction. The magnitude of equation (10) is not only for the oblong modes but also common to all the spheroidal modes except for the breathing mode. Using equation (7), the charging energy associated with phonons is separated from others in H_D as

$$H_\mathrm{D} \approx \sum_k \left(\varepsilon_{\mathrm{D},k} + \frac{eV}{2}\right) c^\dagger_{\mathrm{D},k} c_{\mathrm{D},k} + \frac{e^2}{2C_0}\left(\sum_k c^\dagger_{\mathrm{D},k} c_{\mathrm{D},k}\right)^2 - \beta \frac{u_r}{a}\frac{e^2}{2C_0}\left(\sum_k c^\dagger_{\mathrm{D},k} c_{\mathrm{D},k}\right)^2. \tag{11}$$

β stands for a coupling constant between phonons and electrons, and then the breathing mode phonons are expected to play a dominant role in electron transport in comparison with other modes. On the other hand, the oblong mode has the largest amplitude as compared with other modes, as shown in appendix A, which is also expected to affect predominantly transport properties via the modulation of tunnel resistances. Hence we are devoted to the breathing and oblong vibration modes, hereafter.

Using an isotropic elastic continuum model, we derive the breathing mode (B) and its vibrational spectra in the gold spherical particle with free surface in appendix A. The lowest angular frequency ω_B becomes $\omega_\mathrm{B} = 9.52 \times 10^3/a$ rad s^{-1}, and higher frequencies are approximately harmonics of ω_B, i.e. $\omega_n \approx n\omega_\mathrm{B}$ ($n = 2, 3, \ldots$). The displacement at the particle surface becomes largest for ω_B and decreases for ω_n with increasing n. For $a = 1$ nm, the fundamental frequency becomes $\omega_\mathrm{B}/2\pi = 1.52$ THz and higher phonon frequencies become comparable to or larger than the Debye frequency (3.44 THz). In the frequency region, the elastic continuum model is not suitable to describe vibrations in the solid, and then the phonon frequencies obtained are unreliable except for the fundamental one. The fundamental frequency of the oblong mode (O) is $\omega_\mathrm{O} = 3.24 \times 10^3/a$ rad s^{-1} and the higher modes are approximately harmonics of ω_O. The amplitude of the fundamental frequency is largest among others, and then we expect that the oblong mode phonons at the fundamental frequency affect noticeably the transport in the SET. Considering these, we take account of only the breathing mode phonons at ω_B and the oblong mode phonons at ω_O in this work.

The surface displacement u_r toward the electrodes is expressed in a quantized form by

$$u_r = \kappa_K a(b_K + b_K^\dagger), \tag{12}$$

in terms of the annihilation b_K and creation operators $b_K^\dagger$ of a breathing ($K = \mathrm{B}$) and oblong mode phonons ($K = \mathrm{O}$). In equation (12), κ_K is the ratio of the surface displacement to a, which is evaluated as (equation (A.25))

$$\kappa_\mathrm{B} = 2.33 \times 10^{-22}\frac{1}{a^2} \tag{13}$$

for the breathing mode at ω_B and

$$\kappa_\mathrm{O} = 29.87 \times 10^{-22}\frac{1}{a^2} \tag{14}$$

for the oblong mode at ω_O. Substituting equation (12) into equation (11), we have H_D.

The Hamiltonian H_ph of phonons in the island is

$$H_\mathrm{ph} = \sum_J \hbar\omega_J\left(b_J^\dagger b_J + \tfrac{1}{2}\right), \tag{15}$$

where J stands for a set of quantum numbers given in equation (A.17). The heat bath H_b is modeled by a phonon bath and we assume linear coupling between the phonons in the island and those in the heat bath for $H_\mathrm{ph\text{-}b}$.

We do not take into account the bulk electron–phonon interaction in the island and anharmonic interaction among phonons since they do not contribute to electron tunneling. However, they work for thermal equilibration in the island, whose effects are incorporated below.

3. Canonical transformation

We sort the Hamiltonians into those of the system H_S, environment H_E and interaction H_int:

$$H_\mathrm{S} = H_\mathrm{D} + H_\mathrm{ph} \tag{16}$$

$$H_\mathrm{E} = H_\mathrm{L} + H_\mathrm{R} + H_\mathrm{b} \tag{17}$$

$$H_\mathrm{int} = H_\mathrm{T} + H_\mathrm{ph\text{-}b}. \tag{18}$$

Dealing with H_int as a perturbation, we diagonalize $H_\mathrm{S} + H_\mathrm{E}$ by a canonical transform and modify H_int by the same canonical transformation. In the rest of this work, we investigate individually the phonon effects of the breathing and oblong mode phonons, and then b_K and $b_K^\dagger$ appearing in equation (11) are the operators for either mode of them.

We separate the off-diagonal part H_1 containing u_r in equation (11) from H_S as

$$H_\mathrm{S} = H_0 + \eta H_1, \tag{19}$$

where

$$H_0 = \sum_J \hbar\omega_J\left(b_J^\dagger b_J + \tfrac{1}{2}\right) + \sum_k \left(\varepsilon_{\mathrm{D},k} + \frac{eV}{2}\right) c^\dagger_{\mathrm{D},k} c_{\mathrm{D},k} + \mathcal{E}_C\left(\sum_k c^\dagger_{\mathrm{D},k} c_{\mathrm{D},k}\right)^2 \tag{20}$$

$$H_1 = -(b_K + b_K^\dagger)\mathcal{E}_C\left(\sum_k c^\dagger_{\mathrm{D},k} c_{\mathrm{D},k}\right)^2 \tag{21}$$

$$\eta = \beta\kappa_K. \tag{22}$$

Here $\mathcal{E}_C$ is

$$\mathcal{E}_C = \frac{e^2}{2C_0}. \tag{23}$$

Suitably choosing an operator S as

$$S = \frac{\mathcal{E}_C}{\hbar\omega_K}(b_K - b_K^\dagger)\left(\sum_k c_{\mathrm{D},k}^\dagger c_{\mathrm{D},k}\right)^2, \tag{24}$$

we diagonalize H_S as follows:

$$\begin{aligned}\tilde{H}_\mathrm{S} &= \mathrm{e}^{\eta S} H_\mathrm{S} \mathrm{e}^{-\eta S} \\ &= \sum_J \hbar\omega_J \left(b_J^\dagger b_J + \frac{1}{2}\right) + \sum_k \left(\varepsilon_{\mathrm{D},k} + \frac{eV}{2}\right) c_{\mathrm{D},k}^\dagger c_{\mathrm{D},k} \\ &\quad + \mathcal{E}_C \left(\sum_k c_{\mathrm{D},k}^\dagger c_{\mathrm{D},k}\right)^2 - \eta^2 \frac{\mathcal{E}_C^2}{\hbar\omega_K}\left(\sum_k c_{\mathrm{D},k}^\dagger c_{\mathrm{D},k}\right)^4. \end{aligned} \tag{25}$$

The eigenstate is given by $|\tilde{\Phi}_\mathrm{S}\rangle = |\{n_{\mathrm{D},k}\}, \{m_K\}\rangle$ and the eigenenergy becomes

$$\begin{aligned}E_\mathrm{S} &= \sum_J \hbar\omega_J \left(m_J + \tfrac{1}{2}\right) \\ &\quad + \sum_k \left(\varepsilon_{\mathrm{D},k} + \frac{eV}{2}\right) n_{\mathrm{D},k} + \mathcal{E}_\mathrm{S}(n), \end{aligned} \tag{26}$$

where $n_{\mathrm{D},k}$ is the occupation number of the k-state in the island and m_J is the number of phonons of mode J. n is the total number of extra electrons on the island with respect to the electrically neutral state. The charging energy $\mathcal{E}_\mathrm{S}(n)$ is given by

$$\mathcal{E}_\mathrm{S}(n) = \mathcal{E}_C n^2 - \eta^2 \frac{\mathcal{E}_C^2}{\hbar\omega_K} n^4, \tag{27}$$

where the second term on the right-hand side of equation (27) is due to virtual phonons.

In contrast to H_S, S commutes H_E:

$$[S, H_\mathrm{E}] = 0, \tag{28}$$

and then H_E is unchanged for the canonical transform. Then the eigenstate of the $\tilde{H}_\mathrm{S} + \tilde{H}_\mathrm{E}$ becomes

$$|\tilde{\Psi}\rangle = |\{n_{\mathrm{D},k}\}, \{m_J\}\rangle \otimes |\{n_{\mathrm{L},k}\}, \{n_{\mathrm{R},k}\}, \{m_\mu\}\rangle. \tag{29}$$

$n_{\mathrm{L},k}$, $n_{\mathrm{R},k}$ and m_μ are the occupation numbers of electrons in the source and drain, and the number of phonons of mode μ in the heat bath.

The tunnel Hamiltonian H_T is converted in the same way as H_S and becomes

$$\begin{aligned}\tilde{H}_\mathrm{T} &= \sum_{k,k'} [t_\mathrm{L}^0 c_{\mathrm{L},k}^\dagger c_{\mathrm{D},k'} B + t_\mathrm{L}^{0*} B^\dagger c_{\mathrm{D},k'}^\dagger c_{\mathrm{L},k} \\ &\quad + t_\mathrm{R}^0 c_{\mathrm{R},k}^\dagger c_{\mathrm{D},k'} B + t_\mathrm{R}^{0*} B^\dagger c_{\mathrm{D},k'}^\dagger c_{\mathrm{R},k}], \end{aligned} \tag{30}$$

where

$$B = \mathrm{e}^{\kappa_K(\frac{a}{\lambda} + \beta\frac{\mathcal{E}_C}{\hbar\omega_K})b_K^\dagger + \kappa_K(\frac{a}{\lambda} - \beta\frac{\mathcal{E}_C}{\hbar\omega_K})b_K}. \tag{31}$$

4. Master equation

In order to formulate transport properties such as current and its noise, we introduce a reduced density matrix defined by $\rho_{nn}^{mm}(t) = \mathrm{Tr}[\rho(t)]_{n,m}$, where $m(=m_K)$ is the number of breathing/oblong mode phonons in the island. Considering the case that only the two states with $n = 0$ and 1 are involved in transport, we derive equations of motion of ρ_{nn}^{mm} for each n. Using a von Neumann equation, the master equation yields

$$\dot{\rho}_{00}^{mm} = \sum_{m'} \Gamma(0, m \mid 0, m')\rho_{00}^{m'm'} + \sum_{m'} \Gamma(0, m \mid 1, m')\rho_{11}^{m'm'} \tag{32}$$

$$\dot{\rho}_{11}^{mm} = \sum_{m'} \Gamma(1, m \mid 0, m')\rho_{00}^{m'm'} + \sum_{m'} \Gamma(1, m \mid 1, m')\rho_{11}^{m'm'}. \tag{33}$$

The matrix elements are

$$\begin{aligned}\Gamma(0, m|1, m') &= \sum_{\alpha=\mathrm{L,R}} \gamma_\alpha |\langle m|B|m'\rangle|^2 \left(\frac{C_0}{e^2}\right) \\ &\quad \times F(-\Delta\mu_\alpha + \mathcal{E}_C + \Delta\mu_D + (m' - m)\hbar\omega_K) \end{aligned} \tag{34}$$

$$\begin{aligned}\Gamma(1, m|0, m') &= \sum_{\alpha=\mathrm{L,R}} \gamma_\alpha |\langle m'|B|m\rangle|^2 \left(\frac{C_0}{e^2}\right) \\ &\quad \times F(\Delta\mu_\alpha - \mathcal{E}_C - \Delta\mu_D - (m - m')\hbar\omega_K) \end{aligned} \tag{35}$$

$$\begin{aligned}\Gamma(0, m|0, m') &= -\delta_{m,m'} \sum_{m''} \Gamma(1, m'' \mid 0, m) \\ &\quad - 2\gamma_\infty N(\omega_K)[(m+1)\delta_{m,m'} - m\delta_{m-1,m'}] \\ &\quad - 2\gamma_\infty [N(\omega_K) + 1][m\delta_{m,m'} - (m+1)\delta_{m+1,m'}] \end{aligned} \tag{36}$$

$$\begin{aligned}\Gamma(1, m|1, m') &= -\delta_{m,m'} \sum_{m''} \Gamma(0, m'' \mid 1, m) \\ &\quad - 2\gamma_\infty N(\omega_K)[(m+1)\delta_{m,m'} - m\delta_{m-1,m'}] \\ &\quad - 2\gamma_\infty [N(\omega_K) + 1][m\delta_{m,m'} - (m+1)\delta_{m+1,m'}] \end{aligned} \tag{37}$$

where

$$\gamma_\alpha = (R_\alpha C_0)^{-1}, \tag{38}$$

and $F(x)$ is

$$F(x) = \frac{x}{1 - \mathrm{e}^{-x/k_\mathrm{B}T}}. \tag{39}$$

Here we put

$$\mathcal{E}_\mathrm{S}(1) \approx \mathcal{E}_C, \tag{40}$$

The changes in the chemical potentials are related to the bias voltage as follows:

$$\Delta\mu_\mathrm{L} = \mathrm{eV} \tag{41}$$

$$\Delta\mu_\mathrm{R} = 0 \tag{42}$$

$$\Delta\mu_D = \tfrac{1}{2}\,\mathrm{eV}. \tag{43}$$

The Franck–Condon factor can be computed as

$$\begin{aligned}|\langle m|B|m'\rangle|^2 &= |\langle m|\mathrm{e}^{z_1 b^\dagger - z_2 b}|m'\rangle|^2 \\ &= \mathrm{e}^{-z_1 z_2} z^{2|m-m'|} \frac{p!}{q!}\left[L_p^{|m-m'|}(z_1 z_2)\right]^2, \end{aligned} \tag{44}$$

where

$$z = z_1\,\Theta(m - m') - z_2\,\Theta(m' - m) \tag{45}$$

and

$$z_1 = \kappa_K\left(\beta\frac{\mathcal{E}_C}{\hbar\omega_K} + \frac{a}{\lambda}\right)$$

$$z_2 = \kappa_K \left(\beta \frac{\mathcal{E}_C}{\hbar\omega_K} - \frac{a}{\lambda} \right).$$

$p = \min(m, m')$ and $q = \max(m, m')$, and $L_p^{|m-m'|}$ is the associated Laguerre polynomial. The diagonal elements of equation (44) decay from unity as the product $z_1 z_2$ increases from 0. On the other hand, the off-diagonal ones related to tunneling associated with multi-phonon emission or absorption increase.

Equations (32) and (33) comprise the terms of electron tunneling with or without phonon mediation and the phonon exchange terms with the heat bath in the Lindblad form [28] as seen in equations (36) and (37), where $N(\omega_K)$ is the Bose–Einstein distribution function of phonons in the heat bath at the same frequency as the breathing or oblong mode phonons.

It is convenient to introduce σ_{nn}^{mm} for evaluation of noise properties in the SET [29], which are subject to the following equation of motion:

$$\dot{\sigma}_{00}^{mm} = \sum_{m'} \Gamma(0, m|0, m')\sigma_{00}^{m'm'} + \sum_{m'} \Gamma(0, m|1, m')\sigma_{11}^{m'm'} + \sum_{m'} \Gamma(0, m|1, m')\rho_{11}^{m'm'} \quad (46)$$

$$\dot{\sigma}_{11}^{mm} = \sum_{m'} \Gamma(1, m|0, m')\sigma_{00}^{m'm'} + \sum_{m'} \Gamma(1, m|1, m')\sigma_{11}^{m'm'}, \quad (47)$$

with the initial condition $\sigma_{nn}^{mm}(t = 0) = 0$ for $n = 0, 1$ and $m \geqslant 0$.

We formulate the total charge transferred to the drain within time interval t, using σ_{nn}^{mm}, as

$$\langle Q(t) \rangle = -e \sum_{n,m} \sigma_{nn}^{mm}, \quad (48)$$

and then the current I yields

$$I = -\lim_{t\to\infty} \frac{\langle Q(t) \rangle}{t}. \quad (49)$$

The noise power spectrum $S(0)$ at zero frequency is related to the variance of Q as

$$S(0) = \lim_{t\to\infty} \frac{2}{t} \Delta Q^2(t), \quad (50)$$

and the time derivative of the variance is given in terms of ρ_{nn}^{mm} and σ_{nn}^{mm} by

$$\frac{\mathrm{d}}{\mathrm{d}t} \Delta Q^2 = 2e^2 \sum_{m,m'} \Gamma(0, m|1, m')\sigma_{11}^{m'm'} - e\langle \dot{Q} \rangle - 2\langle Q \rangle \langle \dot{Q} \rangle, \quad (51)$$

where

$$\langle \dot{Q} \rangle = -e \sum_{m,m'} \Gamma(0, m|1, m')\rho_{11}^{m'm'}. \quad (52)$$

The Fano factor is defined by

$$F = \frac{S(0)}{2eI}, \quad (53)$$

using $S(0)$ obtained from equation (51).

Table 1. Parameters used in the numerical evaluation for $a = 1$ nm.

	Breathing mode	Oblong mode
$\omega/2\pi$	1.516 THz	0.515 THz
κ_K	2.426×10^{-4}	29.876×10^{-4}
β	$1 + \frac{a}{2c} = 1.5$	$\frac{a}{2c} = 0.5$
z_1	1.62×10^{-2}	1.97×10^{-1}
z_2	6.517×10^{-3}	7.750×10^{-2}

5. Numerical results

5.1. Temperature in the particle

Phonon emission and absorption induced by electron tunneling are expected to heat up or to cool down the island. The temperature in the island is determined from the distribution of phonon occupation numbers. Then we first examine the distribution of phonon occupation numbers and obtain the island temperature. Considering the particle is put at the midpoint between the electrodes, we put both the characteristic tunneling rates γ_L and γ_R to be γ, and assume $\omega_K \gg \gamma$. At the steady state, i.e. $\dot{\rho}_{nn}^{mm} = 0$, thermal properties depend on the ratio $\frac{\gamma_\infty}{\gamma}$. Then we numerically investigate thermal and transport properties, putting $\gamma_\infty = 0.01\gamma$ in this work for convenience. We solve equations (32) and (33) self-consistently by means of the Runge–Kutta method of fourth order, where we substitute the temperature T in equation (39) by the temperature in the island calculated from the averaged number of phonons discussed below in order to incorporate thermal equilibration among phonons and electrons. Here the bias voltage V is expressed in units of e/C_0, and $VC_0/e = 1$ which is equivalent to $\frac{1}{2}eV = \mathcal{E}_C$ is the threshold bias voltage for tunneling without phonon mediation. The parameters used are given in table 1.

We examined ρ_{nn}^{mm} versus m at $T = 4$ K for various bias voltages from $VC_0/e = 0.97$ to 1.20 and find $\rho_{11}^{mm} \propto \rho_{00}^{mm}$. Figure 2 plots the total phonon occupation probability ρ^{mm} $(=\rho_{00}^{mm} + \rho_{11}^{mm})$ versus m. ρ^{mm} for $VC_0/e \leqslant 0.97$ or $VC_0/e \geqslant 1.20$ decreases exponentially with increasing m, indicating that ρ^{mm} becomes a distribution of a thermal equilibrium state, i.e. the canonical distribution $\rho^{mm} = \mathrm{e}^{-m\hbar\omega_K/k_\mathrm{B}T'}(1 - \mathrm{e}^{-\hbar\omega_K/k_\mathrm{B}T'})$, although the temperature T' in the island is different from that of the environment when phonon-mediated tunneling occurs. Using the Bose–Einstein distribution function, we estimate the temperature T' from the averaged number of phonons $\langle m_\mathrm{O} \rangle [=\mathrm{Tr}(m\rho_{nn}^{mm})]_{K=\mathrm{O}}$ in the island as

$$T' = \frac{\hbar\omega_\mathrm{O}}{k_\mathrm{B}} \frac{1}{\ln\left(\frac{1}{\langle m_\mathrm{O} \rangle} + 1\right)}. \quad (54)$$

T' for $VC_0/e \leqslant 0.97$ agrees with the heat bath temperature, i.e. 4 K, and T' for $VC_0/e \geqslant 1.2$ becomes larger than 4 K, which will be shown below.

The phonon occupation probability does not always become the canonical distribution, however. Figure 2 shows a concave variation of ρ^{mm} in the semi-log scale with respect to m for $0.97 < VC_0/e < 1.2$, manifesting deviation from the canonical distribution. Such a deviation of phonon distribution probability from the canonical distribution is also known

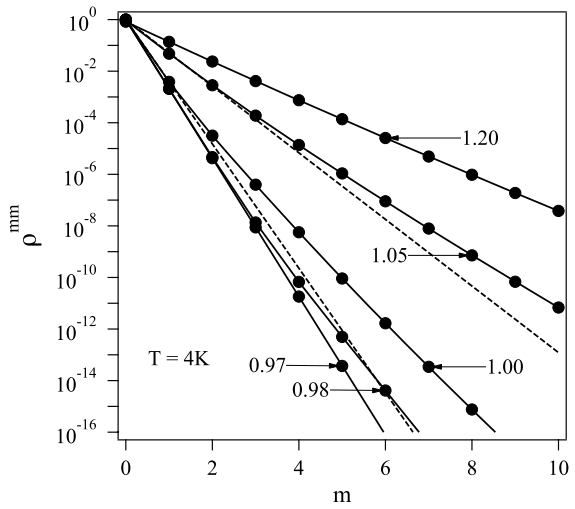

Figure 2. ρ^{mm} versus m at bias voltages from $VC_0/e = 0.97$ to 1.2 for oblong mode phonons. The lines with solid circles indicate ρ^{mm} at each magnitude of VC_0/e. The temperature of the heat bath is set as $T = 4$ K and the thermal dissipation coefficient as $\gamma_\infty = 0.01\gamma$. ρ^{mm} for $VC_0/e = 0.97$ and 1.2 agree with the canonical distribution, while the distribution deviates from the canonical one between the bias voltages. The dashed lines denote the canonical distribution derived from the phonon number for $VC_0/e = 1.00$ and 1.05.

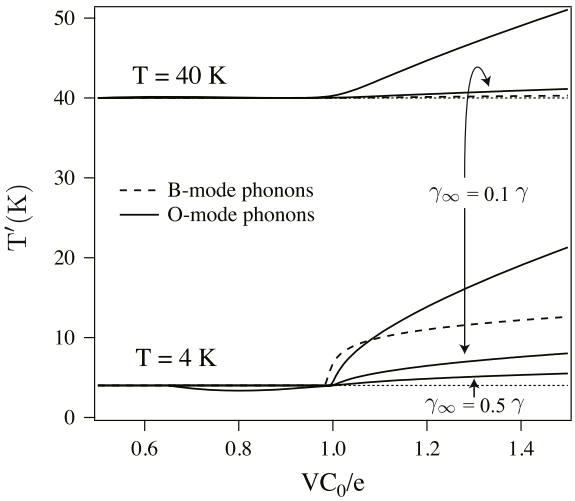

Figure 3. The temperature T' in the nanoparticle versus V at $T = 4$ K for $\gamma_\infty = 0.01\gamma$, 0.1γ and 0.5γ. The data lines of $\gamma_\infty = 0.1\gamma$ and 0.5γ are denoted by arrows. T is the temperature of the heat bath.

to take place in a molecular transistor [3], where electron tunneling mediated by multi-phonon absorption/emission occurs. Indeed, when the multi-phonon absorption/emission processes are artificially suppressed in the present work, the phonon occupation probability becomes the canonical distribution.

The effects of multi-phonon processes on ρ^{mm} do not appear at $VC_0/e \leqslant 0.97$, as mentioned above. In the low bias voltage region, tunneling does not take place and then the phonon distribution is governed by thermal energy exchange between the island and the heat bath, with the distribution becoming the canonical distribution at the heat bath temperature. In the bias voltage region $0.97 < VC_0/e < 1.2$, not only the phonon-absorbed tunneling but also the tunneling associated with phonon emission are possible, even when the bias is below the threshold voltage for phonon emission because of thermal fluctuations in electron energy. These processes affect the distribution of phonon occupation probability; according to the Monte Carlo simulations based on the master equations (32) and (33), for example, at $VC_0/e = 0.99$, tunneling associated with single-phonon emission occurs most frequently when an electron leaves the island, aside from tunneling without phonon mediation. Single-phonon absorption when an electron tunnels onto the island, and two-phonon emission when an electron tunnels off the island, occur at a comparable rate, which is an order of magnitude smaller than the single-phonon emission. Thus the tunneling associated with multi-phonon emission makes the probability of multi-phonon states larger, so that the distribution deviates from the canonical distribution. Phonon-absorbed tunneling might be expected to lead to thermal cooling of the island in the bias region, but the tunneling associated with single-phonon absorption is overcome by the tunneling with two-phonon emission, as mentioned above. As a consequence, the island gains rather than loses energy. Even if the cooling takes place, the coupling to the thermal bath makes the effect small. At a larger bias voltage, $VC_0/e > 1.2$, the number of phonons in the island increases and then the exchange of phonons between the island and the heat bath dominates thermal equilibration. As a consequence, the phonon occupation probability becomes a canonical distribution at temperatures larger than that of the heat bath. From these discussions, it is concluded that the canonical distribution appears when the thermal coupling between the island and the heat bath dominates thermal equilibration. At high heat bath temperature, $N(\omega_K)$ in the heat bath becomes large, enhancing thermal coupling between the island and the heat bath. The canonical distribution of ρ^{mm} appears at. for example, 40 K, even in the bias region $0.97 < VC_0/e < 1.2$. The same effects appear for large thermal coupling γ_∞, since it increases phonon energy exchange between the island and the heat bath.

Because of the phonon occupation probability distinct from the canonical distribution, we define the temperature T' in the island by means of entropy S given by

$$S = -k_{\mathrm{B}} \sum_m \rho^{mm} \log \rho^{mm}. \tag{55}$$

Numerically differentiating S and $\langle m_K \rangle$ with respect to $\{\rho^{mm}\}$ provided that $\sum_m \delta\rho^{mm} = 0$ and using the following thermodynamic definition of temperature:

$$\frac{1}{T'} = \frac{1}{\hbar\omega_K} \frac{\mathrm{d}S}{\mathrm{d}\langle m_K \rangle}, \tag{56}$$

T' is obtained. The resultant T' agrees well with the temperature given by equation (54). The dashed lines in figure 2 denote $\mathrm{e}^{-\hbar\omega_0/k_{\mathrm{B}}T'}$ for $VC/e = 1.00$ and 1.05, which agree with ρ^{mm}_{00} for $m \leqslant 1$ and 2, respectively.

In figure 3, we plot T' versus V at $T = 4$ and 40 K for each case of the breathing and oblong mode phonons, with

$\gamma_\infty = 0.01\gamma$, 0.1γ and 0.5γ. The rate at which T' increases with bias depends on how fast the phonon energy dissipates to the heat bath and becomes small for large γ_∞/γ.

The onset of the temperature increase depends on the phonon modes. The temperature rise begins at a lower bias voltage for the breathing mode than that for the oblong mode because the threshold voltage associated with phonon absorption is lower for the breathing mode; $\omega_B > \omega_O$. Even below the threshold bias for tunneling associated with phonon emission, the island gains phonon energy by phonon emission, as mentioned above. As a consequence, the temperature for the breathing mode rises more steeply at lower bias voltage. Conversely, the increasing rate is larger for the oblong mode than that for the breathing mode, which is seen clearly at the heat bath temperature of $T = 40$ K.

5.2. Current, differential conductance and noise

We plot the total current I and the current I_{ph} only due to phonon-mediated electron tunneling versus V at $T = 4$ K in figure 4. Figure 4(a) shows the results for the breathing mode. The total current I begins to flow at $VC_0/e = 1$ and increases almost linearly with increasing V. On the other hand, I_{ph} arises at $VC_0/e = 1 + \frac{\hbar\omega_B}{\mathcal{E}_C} \approx 1.03$, which is the threshold bias voltage for tunneling associated with single-phonon emission. Because I_{ph} amounts, at most, to 0.004% of the total current, the signature of phonon effects on I is obscured. Figure 4(b) plots I and I_{ph} due to the oblong mode. I_{ph} begins to arise at $VC_0/e = 1 + \frac{\hbar\omega_O}{\mathcal{E}_C} \approx 1.01$ and increases nonlinearly with respect to V. Although I_{ph} is three orders of magnitude larger than that for the breathing mode, it is not yet large enough to cause apparent modifications on the total current I.

In order to resolve the subtle phonon effects on the current, we look at the differential conductance σ of the total current, the Fano factor F and σ_{ph} only due to phonon-mediated tunneling,. We expect steps in σ due to additional conductance channels arising from phonon emission. As for the Fano factor, a drastic increase in F is anticipated when the phonon-mediated tunneling begins to occur in addition to the tunneling without phonon mediation. Figure 5 plots σ, σ_{ph} and F at 4 K for (a) the breathing and (b) the oblong modes, which show no notable changes in σ and F, contrary to the expectation for both cases.

There is a prominent difference in the bias voltage dependence of σ_{ph} between the two cases; σ_{ph} for the breathing mode decays gradually with increasing bias after the abrupt increase in magnitude, similarly to σ. The similarity indicates that I_{ph} is predominantly owing to a single channel, i.e. tunneling associated with single-phonon emission. In contrast, σ_{ph} for the oblong mode phonons continues to increase with increasing the bias, reflecting the nonlinear increase in I_{ph} with respect to the bias. Considering that the multi-phonon-mediated tunneling makes the phonon number probability of the oblong mode deviate from the canonical distribution more than that of the breathing mode and that I_{ph} for the oblong mode is three orders of magnitude larger than that for the breathing mode, we speculate that I_{ph} for the oblong mode results from superposition of currents owing to multi-phonon-mediated tunneling while I_{ph} for the breathing mode

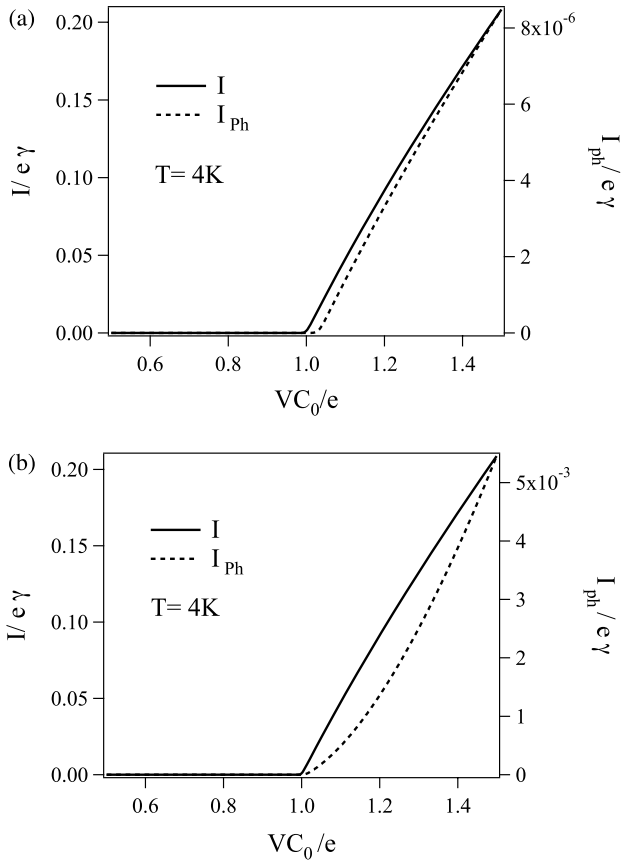

Figure 4. The total current I and phonon-mediated current I_{ph} for (a) the breathing and (b) oblong modes versus V at $T = 4$ K.

phonons is due to tunneling associated with single-phonon emission. If so, characteristic steps in σ_{ph} are expected in figure 5(b), although σ_{ph} varies smoothly with increasing V.

To illustrate the contribution of multi-phonon-mediated tunneling to the transport, we investigate the second derivative of current with respect to V. Figure 6(a) shows $\frac{d^2I}{dV^2}$ and $\frac{d^2I_{ph}}{dV^2}$ versus V for the breathing mode at various heat bath temperatures from 4 to 40 K. $\frac{d^2I}{dV^2}$ has a main peak at $VC_0/e = 1$, which lowers and broadens with increasing temperature. On the other hand, at $T = 4$ K, $\frac{d^2I_{ph}}{dV^2}$ shows sidebands at $VC_0/e = 1 \pm 0.03$ due to single-phonon absorption ($-$) and emission ($+$). These two peaks are too small to be resolved in $\frac{d^2I}{dV^2}$. As the temperature increases, the peak due to the phonon absorption becomes larger and broadens, while the peak due to phonon emission flattens. The peaks eventually merge at $T \geqslant 20$ K and the effects of phonon absorption and emission become indistinguishable above 20 K.

Figure 6(b) plots $\frac{d^2I}{dV^2}$ and $\frac{d^2I_{ph}}{dV^2}$ versus V for the oblong mode, and there are sidebands in $\frac{d^2I_{ph}}{dV^2}$ indicating single-phonon absorption and emission at $VC_0/e = 1 \pm 0.01$. Because the two sidebands are close in energy, the peak corresponding to phonon absorption is only just resolved at low temperature. The two peaks merge with increasing temperature and become indistinguishable at $T = 20$ K. Although we expected other sidebands associated with multi-phonon absorption/emission

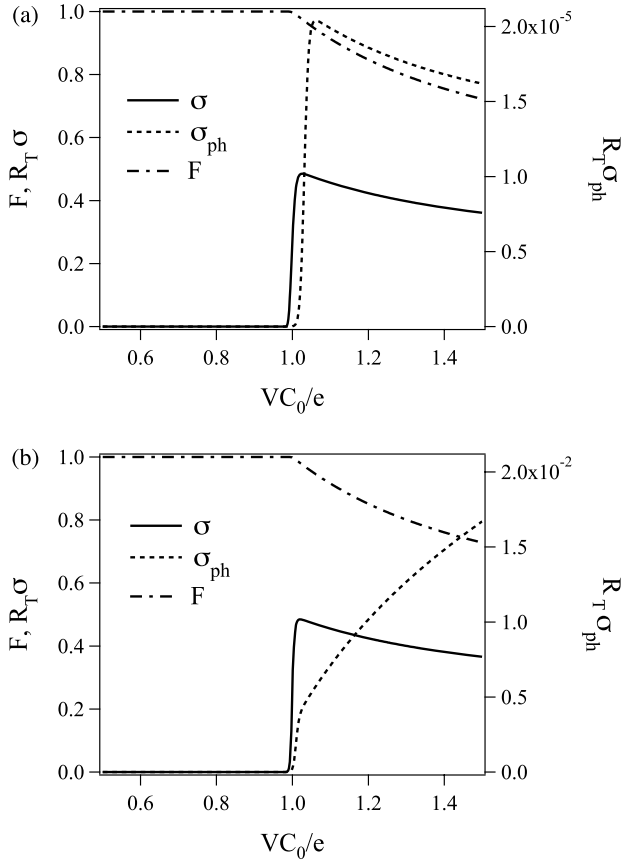

Figure 5. The differential conductance σ of the total current I and $\sigma_{\rm ph}$ of phonon-mediated current $I_{\rm ph}$ together with the Fano factor F for (a) the breathing and (b) oblong modes versus V at $T = 4$ K. $R_{\rm T}$ is the tunnel resistance between the particle island and leads.

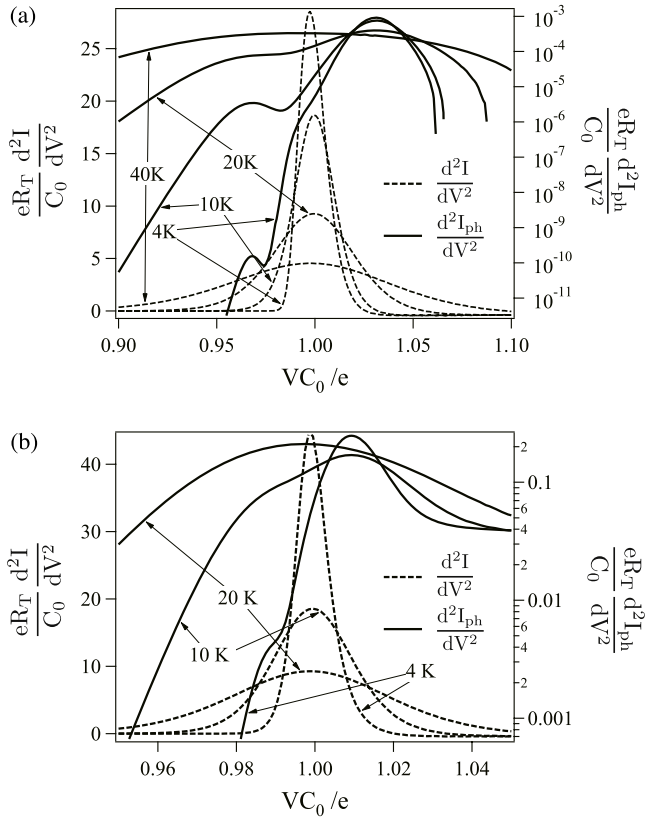

Figure 6. The second differential conductance of the total current $\frac{{\rm d}^2 I}{{\rm d}V^2}$ and that of the phonon-mediated current $\frac{{\rm d}^2 I_{\rm ph}}{{\rm d}V^2}$ versus V at 4 K for (a) the breathing mode and (b) oblong mode.

at, for example, $VC_0/e = 1.00 \pm 0.02$, no evidence of extra peaks was found in $\frac{{\rm d}^2 I_{\rm ph}}{{\rm d}V^2}$, indicating that the nonlinear increase in $I_{\rm ph}$ for the oblong mode is not primarily the result of multi-phonon-mediated tunneling.

To investigate this situation, we consider the current in the steady state that may be described as

$$I = e\sum_m [\Gamma(1, m|0, m) + \Gamma(1, m+1 \mid 0, m) + \Gamma(1, m-1 \mid 0, m)]\rho_{00}^{mm}, \tag{57}$$

which is derived from the master equations (32) and (33) provided that $\langle \dot{n} \rangle = 0$. The relevant phonon-mediated component $I_{\rm ph}$ is

$$I_{\rm ph} = e\sum_m [\Gamma(1, m+1|0, m) + \Gamma(1, m-1|0, m)]\,\rho_{00}^{mm}. \tag{58}$$

The matrix elements for single-phonon-mediated tunneling can be approximated as

$$\Gamma(1, m+1|0, m) \approx (m+1)\Gamma(1, 1 \mid 0, 0) \tag{59}$$

$$\Gamma(1, m-1|0, m) \approx m\Gamma(1, 0 \mid 0, 1), \tag{60}$$

since $\frac{p!}{q!}[L_p^1(z)]^2 \approx \frac{p!}{q!}(p+1)^2$ for small z in equation (44). Expressing ρ_{nn}^{mm} by the product of the electronic part ρ_{nn} and the canonical distribution:

$$\rho_{nn}^{mm} = \rho_{nn}\frac{{\rm e}^{-m\hbar\omega_K/k_{\rm B}T'}}{Z}, \tag{61}$$

where

$$Z = \frac{1}{1 - {\rm e}^{-\hbar\omega_K/k_{\rm B}T'}}, \tag{62}$$

$I_{\rm ph}$ yields

$$I_{\rm ph} \approx e\sum_m [(m+1)\Gamma(1, 1|0, 0) + m\Gamma(1, 0|0, 1)]\,\rho_{00}^{mm} = e\Gamma(1, 1|0, 0)\rho_{00} + e\langle m_K\rangle[\Gamma(1, 1|0, 0) + \Gamma(1, 0|0, 1)]\rho_{00}. \tag{63}$$

The Γs increase linearly with respect to the bias, and the number of phonons $\langle m_K \rangle$ also increases with increasing bias because of phonon emission. As a consequence, if ρ_{00} is almost constant the second term of equation (63) increases nonlinearly with increasing bias, resulting in the nonlinear increase in $I_{\rm ph}$.

The magnitude in $\langle m_K \rangle$ depends on both the electron–phonon coupling and the thermal resistance between the island and heat bath. Hence, the nonlinear behavior depends on how rapidly $\langle m_K \rangle$ grows with bias. The difference in the bias dependence of $I_{\rm ph}$ between the breathing and oblong modes can be estimated by considering the situation where the first term in equation (63) is equal to the size of the second

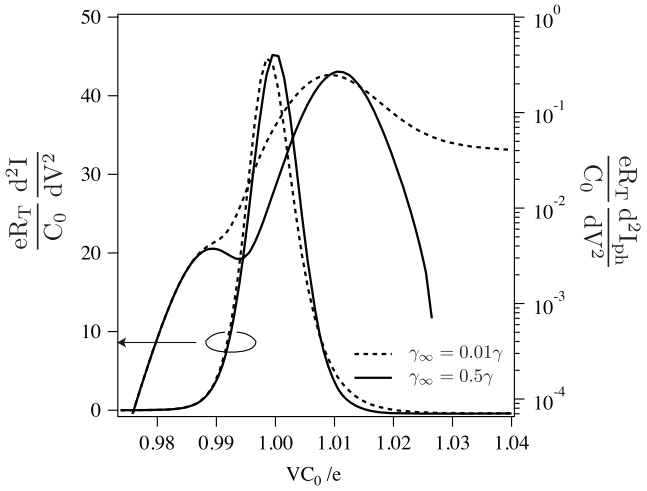

Figure 7. The second differential conductance of the total current $\frac{d^2I}{dV^2}$ and that of the phonon-mediated current $\frac{d^2I_{ph}}{dV^2}$ versus V at 4 K for the oblong mode. The dotted and solid lines indicate the results for $\gamma_\infty = 0.01\gamma$ and 0.5γ, respectively.

term because of the increase in $\langle m_K \rangle$. In this case, from equation (63) $\langle m_K \rangle$ becomes equal to the ratio

$$\langle m_K \rangle = \frac{\Gamma(1,1|0,0)}{\Gamma(1,1|0,0) + \Gamma(1,0|0,1)}. \tag{64}$$

The right-hand side of equation (64) becomes 0 at the threshold bias voltage for single-phonon emission and saturates to be 0.13 for the oblong mode and 0.11 for the breathing mode at very large bias (see appendix B). Because saturation happens quickly, the ratio becomes ≈0.1 even at $\frac{C_o V}{e} = 1.1$ where the nonlinear behavior of I_{ph} is confirmed for the oblong mode in figure 4(b). Supposing $\langle m_K \rangle = 0.1$, the temperature T_K of the island for the breathing and oblong modes is estimated from equation (54) to be $T_B = 30.4$ K and $T_O = 10.3$ K, respectively.

As shown in figure 3, the temperature of the island for the oblong mode becomes larger than 10 K at $VC_0/e > 1.1$. In contrast, the temperature for the breathing mode does not reach 30 K in the bias region studied. This argument shows that, as a result of the bias dependence of $\langle m_K \rangle$, I_{ph} for the oblong mode increases nonlinearly, while that for the breathing mode increases linearly over the parameter range considered. The difference in I_{ph} between the oblong and breathing modes also leads to the difference in the magnitude and bias dependence of $\frac{d^2I_{ph}}{dV^2}$ at $VC_0/e > 1.04$, as seen in figures 6(a) and (b).

From the discussion, we can assess the behavior of $\frac{d^2I_{ph}}{dV^2}$ at $VC_0/e > 1.04$ for the oblong mode at large γ_∞. The large γ_∞ reduces $\langle m_O \rangle$, which is expected to lead to a linear increase in I_{ph}, like the breathing mode. Figure 7 compares $\frac{d^2I_{ph}}{dV^2}$ for the oblong mode versus V between $\gamma_\infty = 0.01\gamma$ and 0.5γ. $\frac{d^2I_{ph}}{dV^2}$ for $\gamma_\infty = 0.5\gamma$ becomes negative at $VC_0/e = 1.026$, similar to that of the breathing mode, confirming that the nonlinear increase in I_{ph} is a thermal effect.

6. Summary and conclusion

We have discussed how phonons associated with the island of an SET influence the electron transport of the device. We have formulated the tunnel Hamiltonian to incorporate the changes in the capacitances and tunnel resistances caused by phonons. Based on this result, we set up the master equations for the density matrix and formulate the current, differential conductance and the Fano factor.

Applying the model to an ideal SET containing a spherical gold particle 1 nm in radius, we calculated the effects of the breathing and oblong mode phonons on the thermal properties of the island and on the electron transport. Phonon emission associated with tunneling raises the temperature in the island and multi-phonon emission makes the phonon occupation number in the island deviate from the canonical distribution even at steady state in the bias region close to the tunneling threshold. The current through the SET is dominated by tunneling without phonon mediation, with the differential conductance and the Fano factor showing little noticeable change due to phonons. The second derivative of the phonon-mediated current exhibits peaks associated with single-phonon absorption and emission similar to phonon signatures found by inelastic electron energy spectroscopy [2] in other systems. In the system studied, peaks associated with multi-phonon emission are smeared. We conclude that the dominant effect of the dynamic deformation of the particle island induced by phonons is on the thermal properties of the island rather than the electronic properties of the SET. Only the molecular vibrations such as vibrons lead to the vivid signatures of the vibrations of the island on the transport [1–8].

Acknowledgments

This work is supported in part by a grant-in-aid for scientific research from the Ministry of Education, Culture, Sports, Science and Technology of Japan (grant nos 1965106507, 20246094 and 21560002).

Appendix A. Acoustic phonons in a particle

We illustrate acoustic phonon modes in the spherical particle with an isotropic elastic continuum model [30, 31]. It is shown that there are spheroidal and toroidal modes. Using the normal modes, we formulate the quantized surface displacement u_r, which appears in equation (6).

The elastic wave equation in the isotropic medium yields

$$\rho\ddot{\mathbf{u}}(\mathbf{r},t) = (\lambda+2\mu)\nabla[\nabla\cdot\mathbf{u}(\mathbf{r},t)] - \mu\nabla\times[\nabla\times\mathbf{u}(\mathbf{r},t)], \tag{A.1}$$

where ρ, λ and μ are the mass density and the Lamé coefficients, respectively. We formulate the displacement vector $\mathbf{u}(\mathbf{r},t)$, using a scalar and two vector potentials as

$$\mathbf{u}(\mathbf{r},t) = \nabla\phi_1 + \nabla\times\mathbf{\Phi}_2 + \nabla\times\nabla\times\mathbf{\Phi}_3. \tag{A.2}$$

The first term on the right-hand side of equation (A.2) represents the longitudinal acoustic wave component and the other two terms those of the perpendicularly polarized

transverse waves. According to the spherical shape, we express the vector potentials in the spherical coordinates as

$$\mathbf{\Phi}_\alpha = (r, 0, 0)\phi_\alpha, \tag{A.3}$$

for $\alpha = 2$ and 3. Putting equation (A.3) into (A.2), we have the following scalar wave equation for each potential function ϕ_α:

$$\left(\nabla^2 - \frac{1}{c_\alpha^2}\frac{\partial^2}{\partial t^2}\right)\phi_\alpha = 0, \tag{A.4}$$

where c_α is the sound velocity given by

$$c_\alpha^2 = [(\lambda + \mu)\delta_{\alpha,1} + \mu]/\rho. \tag{A.5}$$

The potential functions ϕ_αs are given, in spherical coordinates, by

$$\phi_\alpha(\mathbf{r}, t) = \sum_{l=0}^{\infty}\sum_{m=-l}^{l} A_\alpha^{l,m} j_l(k_\alpha r) P_l^{|m|}(\cos\theta)\mathrm{e}^{-\mathrm{i}m\phi}\mathrm{e}^{-\mathrm{i}\omega t}, \tag{A.6}$$

where j_l is the spherical Bessel function of lth order and the wavenumbers k_αs satisfy the following dispersion relations:

$$\omega = k_1 c_1 = k_2 c_2 = k_3 c_3. \tag{A.7}$$

$P_l^{|m|}$ is the associated Legendre polynomials and m is an integer within the region $-l \leqslant m \leqslant l$. $A_\alpha^{l,m}$s are the coefficients of the potential functions, which are determined below.

Applying the stress-free condition on the particle surface, we obtain two types of phonon modes in the particle; spheroidal and toroidal [30, 31]. The former is composed of ϕ_1 and $\mathbf{\Phi}_3$, having the radial component of displacement, while the latter owing to $\mathbf{\Phi}_2$ does not have the component. The eigenvalue equation for the spheroidal modes becomes for given (l, m)

$$\begin{aligned} &2j_{l+1}(\xi)\frac{\xi}{\eta^2}\left\{1 + \frac{(l-1)(l+2)}{\eta}\left[\frac{j_{l+1}(\eta)}{j_l(\eta)} - \frac{l+1}{\eta}\right]\right\} \\ &\quad + j_l(\xi)\left\{-\frac{1}{2} + \frac{(l-1)(2l+1)}{\eta^2}\right. \\ &\quad \left. + \frac{1}{\eta}\left[1 - \frac{2l(l-1)(l+2)}{\eta^2}\right]\frac{j_{l+1}(\eta)}{j_l(\eta)}\right\} = 0, \end{aligned} \tag{A.8}$$

where $\xi = k_1 a$ and $\eta = k_3 a$, respectively. There is the relation between ξ and η from equation (A.7) as

$$\eta = \frac{c_1}{c_3}\xi, \tag{A.9}$$

so that equation (A.8) becomes the equation with respect to only ξ. Although equation (A.8) gives the spectra of spheroidal modes for a couple of parameters (l, m), equation (A.8) is actually independent of m, and then the spheroidal modes are degenerate by $2l + 1$. Hereafter we express an eigenvalue by $\xi_{l,n}(\equiv k_{1,l,n}a = \omega_{l,n}^{\mathrm{S}}a/c_1)$ for a given l, where n indicates the nth solution of equation (A.8). Then, the spheroidal mode is formulated as

$$\begin{aligned} \mathbf{u}_{l,m,n}^{\mathrm{S}}(\mathbf{r}, t) &= A_1^{l,m,n}\{\nabla[j_l(k_{1,l,n}r)P_l^{|m|}(\cos\theta)\mathrm{e}^{-\mathrm{i}m\phi}] \\ &\quad + \alpha(l, n)\nabla\times\nabla\times[(r, 0, 0)j_l(k_{3,l,n}r) \\ &\quad \times P_l^{|m|}(\cos\theta)\mathrm{e}^{-\mathrm{i}m\phi}]\}\mathrm{e}^{-\mathrm{i}\omega_{l,n}^{\mathrm{S}}t}, \end{aligned} \tag{A.10}$$

where the coefficients $A_1^{l,m,n}$ and $\alpha(l)$ are determined from the following normalization condition of the spheroidal mode:

$$\int_V |\mathbf{u}_{l,m,n}^{\mathrm{S}}(\mathbf{r}, t)|^2\,\mathrm{d}V = 1. \tag{A.11}$$

The coefficients become

$$\begin{aligned} A_1^{l,m,n} &= \left[\frac{K_1(l, n)}{k_{1,l,n}} + \frac{\alpha^2(l, n)l(l+1)K_3(l, n)}{k_{3,l,n}}\right]^{-1/2} \\ &\quad \times [2I(l, m)\pi]^{-1/2}, \end{aligned} \tag{A.12}$$

$$I(l, m) = \frac{2(l + |m|)!}{(l - |m|)!(2l + 1)!}, \tag{A.13}$$

$$\begin{aligned} K_1(l, n) &= \int_0^{\xi_{l,n}}\left[\frac{\partial}{\partial\xi}j_l(\xi)\right]^2\xi^2\,\mathrm{d}\xi + l(l+1) \\ &\quad \times \int_0^{\xi_{l,n}} j_l^2(\xi)\,\mathrm{d}\xi, \end{aligned} \tag{A.14}$$

$$\begin{aligned} K_3(l, n) &= \int_0^{\eta_{l,n}}\left[\left(\frac{\partial}{\partial\xi} + \frac{1}{\xi}\right)j_l(\xi)\right]^2\xi^2\,\mathrm{d}\xi + l(l+1) \\ &\quad \times \int_0^{\eta_{l,n}} j_l^2(\xi)\,\mathrm{d}\xi, \end{aligned} \tag{A.15}$$

and

$$\alpha(l, n) = \frac{2(l-1)j_l(\xi_{l,n}) - 2\xi_{l,n}j_{l+1}(\xi_{l,n})}{[\eta_{l,n}^2 - 2(l^2-1)]j_l(\eta_{l,n}) - 2\eta_{l,n}j_{l+1}(\eta_{l,n})}. \tag{A.16}$$

The toroidal modes are obtained in the same way as the spheroidal modes.

Using annihilation $a_{l,m,n}^{Q}$ and creation operators $a_{l,m,n}^{Q\dagger}$ of phonons, we formulate the phonon field as

$$\begin{aligned} \mathbf{u}(\mathbf{r}) &= \sum_{Q=\mathrm{S,T}}\sum_{l=0}^{\infty}\sum_{m=-l}^{l}\sum_{n=1}^{\infty}\left(\frac{\hbar}{2\rho\omega_{l,n}^{Q}}\right)^{1/2} \\ &\quad \times \left[a_{l,m,n}^{Q}\mathbf{u}_{l,m,n}^{Q}(\mathbf{r}) + \mathrm{H.c.}\right] \end{aligned} \tag{A.17}$$

in the Schrödinger picture, where Q specifies the spheroidal (S) or toroidal modes (T). We note here that a set of quantum numbers J represents (Q, l, m, n) in the Hamiltonian H_{ph} of phonons in the particle (equation (15)).

In this work, we pay special attention to breathing (B) and oblong (O) modes, belonging to the spheroidal modes. Putting $l = 0$ and $m = 0$, the spheroidal modes become the breathing modes with amplitude of azimuthal symmetric, showing breathing motion. The spheroidal modes for $l = 2$ and $m = 0$ exhibit oblong vibrations, whose vibration spectra contain the lowest vibration frequency among all the spheroidal modes.

The eigenvalue equation (A.8) for the spheroidal modes reduce for the breathing mode to

$$4j_1(\xi)\frac{\xi}{\eta^2} - j_0(\xi) = 0. \tag{A.18}$$

Solving numerically equations (A.8) and (A.18), we obtain the eigenfrequencies. For gold, ξ and η are related by

$$\eta = 2.66\xi \tag{A.19}$$

Table A.1. Dimensionless wavenumbers ξ of breathing mode waves in a gold particle.

l	$n=1$	2	3	4	5
0	···	···	2.939	6.191	9.364
1	···	1.535	2.792	3.996	4.376
2	0.999	1.994	3.303	4.537	5.574

from the mass density $\rho = 19.3$ g cm^{-3} and sound velocities $c_1 = 3.24\times10^3$ m s^{-1} and $c_3 = 1.22\times10^3$ m s^{-1}. Substituting equation (A.19) into (A.18), the eigenfrequencies $\{\xi_{0,n}\}$ are numerically obtained from equation (A.18), which are shown in table A.1.

The fundamental frequency $\omega_{\rm B}$ becomes, for $a = 1$ nm,

$$\omega_{\rm B} = 2\pi \times 1.52 \times 10^{12} \text{ rad s}^{-1} \tag{A.20}$$

and higher frequencies ω_n $(n = 2, 3, \ldots)$ are found, from table A.1, to be approximately harmonics of $\omega_{\rm B}$:

$$\omega_n \approx n\omega_{\rm B}. \tag{A.21}$$

However, ω_n $(n \geqslant 2)$ becomes comparable to or larger than the Debye frequency. In the frequency region, the elastic continuum model cannot describe the particle vibrations correctly, so that the obtained phonon frequencies $\{\omega_n\}(n \geqslant 2)$ become unreliable for the particle size. Table A.1 also shows the spectra of oblong vibrational modes, whose fundamental eigenfrequency is the smallest among the all the spheroidal modes. Although the harmonics being lower than the Debye frequency are considered to be valid, we pay attention only to the breathing and oblong modes of fundamental frequency $\omega_{\rm B}$ and $\omega_{\rm O}$ in this work as representative modes.

The phonon field only due to the phonon mode of interest at $\omega_{\rm K}(K = {\rm B}, {\rm O})$ yields

$$\mathbf{u}_K(\mathbf{r}) = \left(\frac{\hbar}{2\rho\omega_K}\right)^{1/2} \mathbf{u}_K(\mathbf{r})(b_K + b_K^\dagger). \tag{A.22}$$

For the breathing mode, $b_{\rm B} \equiv a^{\rm S}_{0,0,1}$ and $b_{\rm B}^\dagger \equiv a^{{\rm S}\dagger}_{0,0,1}$. $\mathbf{u}_{\rm B} \equiv \mathbf{u}^{\rm S}_{0,0,1}(\mathbf{r})$ has only the radial component, which becomes

$$[\mathbf{u}^{\rm S}_{0,0,1}(\mathbf{a})]_r = \frac{0.435}{a^{3/2}}. \tag{A.23}$$

For the oblong mode, $b_{\rm O} \equiv a^{\rm S}_{2,0,1}$ and $b_{\rm O}^\dagger \equiv a^{{\rm S}\dagger}_{2,0,1}$. $\mathbf{u}_{\rm O} \equiv \mathbf{u}^{\rm S}_{2,0,1}(\mathbf{r})$ and the radial component varies as $\cos\theta$. The amplitude yields

$$[\mathbf{u}^{\rm S}_{2,0,1}(\mathbf{a})]_r = \frac{3.252}{a^{3/2}}, \tag{A.24}$$

at $\theta = 0$.

Using the result, the ratio κ_K of the surface displacement to the radius for the breathing mode becomes

$$\kappa_{\rm B} = 2.331 \times 10^{-22}\frac{1}{a^2}, \tag{A.25}$$

and that for the oblong mode

$$\kappa_{\rm O} = 29.876 \times 10^{-22}\frac{1}{a^2}. \tag{A.26}$$

Using κ_K, the displacement in the radial component u_r at the surface, which appeared in equation (6), yields

$$u_r = \kappa_K a(b_K + b_K^\dagger). \tag{A.27}$$

Here equation (A.27) gives the surface amplitude at $\theta = 0$ for the oblong mode.

Appendix B

The following ratio between the two Γs at low temperature is simplified as follows:

$$\begin{aligned}\frac{\Gamma(1,0|0,1)}{\Gamma(1,1|0,0)} &\approx A_K \frac{F(\frac{eV}{2} - \varepsilon_C + \hbar\omega_K)}{F(\frac{eV}{2} - \varepsilon_C - \hbar\omega_K)} \\ &\approx A_K \frac{\frac{C_0V}{e} - 1 + \frac{\hbar\omega_K}{\varepsilon_C}}{\frac{C_0V}{e} - 1 - \frac{\hbar\omega_K}{\varepsilon_C}},\end{aligned} \tag{B.1}$$

where

$$A_K = \left(\frac{z_1}{z_2}\right)^2. \tag{B.2}$$

Putting equation (B.1) into equation (64), the right-hand side yields

$$\frac{\Gamma(1,1|0,0)}{\Gamma(1,1|0,0) + \Gamma(1,0|0,1)} = \frac{1}{1 + A_K \frac{\frac{C_0V}{e} - 1 + \frac{\hbar\omega_K}{\varepsilon_C}}{\frac{C_0V}{e} - 1 - \frac{\hbar\omega_K}{\varepsilon_C}}}. \tag{B.3}$$

In the bias region $\frac{C_0V}{e} > 1 + \frac{\hbar\omega_K}{\varepsilon_C}$, the magnitude varies from 0 to $\frac{1}{1+A_K}$ with increasing bias. The saturated magnitudes are 0.11 for the breathing mode and 0.13 for the oblong mode. Here the coefficients $A_{\rm B}$ and $A_{\rm O}$ are

$$A_{\rm B} = 8.03 \tag{B.4}$$

$$A_{\rm O} = 6.46. \tag{B.5}$$

Since the phonon energy is small in comparison with ε_C:

$$\frac{\hbar\omega_{\rm B}}{\varepsilon_C} = 0.03 \tag{B.6}$$

$$\frac{\hbar\omega_{\rm O}}{\varepsilon_C} = 0.01, \tag{B.7}$$

Equation (B.3) rapidly saturates and becomes approximately 0.1 at $VC_0/e = 1.1$ where the nonlinear dependence of $I_{\rm ph}$ is seen for the oblong mode in figure 4(b).

References

[1] Galperin M, Ratner M A and Nitzan A 2007 *J. Phys.: Condens. Matter* **19** 103201
[2] Galperin M, Nitzan A and Ratner M A 2008 *Phys. Rev.* B **78** 15320
[3] Mitra A, Aleiner I and Millis A J 2004 *Phys. Rev.* B **69** 245302
[4] Boese D and Schoeller H 2001 *Europhys. Lett.* **54** 668
[5] Braig S and Flensberg K 2003 *Phys. Rev.* B **68** 205324
[6] Wegewijs M R and Nowack K C 2005 *New J. Phys.* **7** 239
[7] Koch J and von Oppen F 2005 *Phys. Rev. Lett.* **94** 206804
[8] Koch J, Semmelhack M, von Oppen F and Nitzan A 2006 *Phys. Rev.* B **73** 155306

[9] Bates A D, Callen B P, Cooper J M, Cosstick R, Geary C, Glidle A, Jaeger L, Pearson J L, Proupín-Pérez M, Xu C and Cumming D R S 2006 *Nano Lett.* **6** 445
[10] Gorelik L Y, Isacsson A, Voinova M V, Kasemo B, Shekhter R I and Jonson M 1998 *Phys. Rev. Lett.* **80** 4526
[11] Armour A D and MacKinnon A 2002 *Phys. Rev.* B **66** 035333
[12] Nishiguchi N 2002 *Phys. Rev.* B **65** 035403
[13] Shekhter R I, Galperin Yu, Gorelik L Y, Isacsson A and Jonson M 2003 *J. Phys.: Condens. Matter* **15** R441
[14] Novotny T, Donarini A and Jauho A-P 2003 *Phys. Rev. Lett.* **90** 256801
[15] Pistolesi F 2004 *Phys. Rev.* B **69** 245409
[16] Fedorets D, Gorelik L Y, Shekhter R I and Jonson M 2004 *Phys. Rev. Lett.* **92** 166801
[17] Flindt C, Novotný T and Jauho A-P 2005 *Europhys. Lett.* **69** 475
[18] Johansson J R, Mourokh L G, Smirnov A Yu and Nori F 2008 *Phys. Rev.* B **77** 035428
[19] Nishiguchi N 2008 *Phys. Rev.* B **78** 085407
[20] Koenig D R, Weig E M and Kotthaus J P 2008 *Nat. Technol.* **3** 482
[21] Armour A D, Blencowe M P and Schwab K C 2002 *Phys. Rev. Lett.* **88** 148301
[22] Blencowe M P 2004 *Phys. Rep.* **395** 159
[23] Knobel R and Cleland A N 2003 *Nature* **424** 291
[24] LaHaye M D, Buu O, Camarota B and Schwab K C 2004 *Science* **304** 74
[25] Savelév S, Hu X and Nori F 2006 *New J. Phys.* **8** 105
[26] Cheng D K 1989 *Field and Wave Electromagnetics* 2nd edn (Reading, MA: Addison-Wesley) pp 172–4
[27] Pólya G and Szegö G 1951 *Isoperimetric Inequalities in Mathematical Physics: Annals of Mathematical Studies* (Princeton, NJ: Princeton University Press)
[28] Lindblad G 1976 *Commun. Math. Phys.* **48** 119
[29] Elattari B and Gurvitz S A 2002 *Phys. Lett.* A **292** 289
[30] Love A E H 1944 *A Treatise on the Mathematical Theory of Elasticity* (New York: Dover) chapter 12
[31] Nakayama T and Nishiguchi N 1981 *Phys. Rev.* B **24** 6421